Vrije Universiteit Brussel

The time-varying effect of thiourea on the copper electroplating process with industrial copper concentrations

Collet, Thomas Marcel; Wouters, Benny; Hallemans, Noel; Ramharter, Kristof ; Lataire, John; Hubin, Annick

Published in:
Electrochimica Acta

Publication date:
2022

Document Version:
Accepted author manuscript

Link to publication

Citation for published version (APA):
Collet, T. M., Wouters, B., Hallemans, N., Ramharter, K., Lataire, J., & Hubin, A. (2022). The time-varying effect of thiourea on the copper electroplating process with industrial copper concentrations. *Electrochimica Acta*, *437*, 1-12. [141412].

Copyright
No part of this publication may be reproduced or transmitted in any form, without the prior written permission of the author(s) or other rights holders to whom publication rights have been transferred, unless permitted by a license attached to the publication (a Creative Commons license or other), or unless exceptions to copyright law apply.

Take down policy
If you believe that this document infringes your copyright or other rights, please contact openaccess@vub.be, with details of the nature of the infringement. We will investigate the claim and if justified, we will take the appropriate steps.

Download date: 18. Sep. 2023

Electrochimica Acta 437 (2023) 141412

Contents lists available at ScienceDirect

Electrochimica Acta

journal homepage: www.journals.elsevier.com/electrochimica-acta

The time-varying effect of thiourea on the copper electroplating process with industrial copper concentrations

Thomas Collet [a,*], Benny Wouters [a], Noël Hallemans [b,c], Kristof Ramharter [d], John Lataire [b], Annick Hubin [a]

[a] Vrije Universiteit Brussel, Research Group Electrochemical and Surface Engineering, Pleinlaan 2, 1050 Brussels, Belgium
[b] Vrije Universiteit Brussel, Research Group Fundamental electricity and Instrumentation, Pleinlaan 2, 1050 Brussels, Belgium
[c] University of Warwick, WMG, Coventry CV4 7AL, United Kingdom
[d] Aurubis Olen N.V., Watertorenstraat 35, 2250 Olen, Belgium

ARTICLE INFO

Keywords:
Electrorefining
Copper reduction
Thiourea
Operando ORP-EIS
Time-varying impedance

ABSTRACT

Electrorefining is the process of choice to purify several metals, among which is copper. A crucial process parameter in electrorefining, and electroplating in general, is the additive activity. Several additives are introduced to the electrolyte to ensure a morphological smooth copper deposit. Thiourea is a crucial but complex additive used in copper electrorefining, it is known to degenerate and both the reaction product as thiourea itself can complex with the copper ions. Unfortunately, time dependent additive studies and mechanistic knowledge of the effect of aged electrolyte on the cathodic part of the electrorefining process are scarce. In this work, operando Odd Random Phase Electrochemical Impedance Spectroscopy (ORP-EIS) is used to study the electrochemistry of a copper plating system containing industrial copper concentrations. The approach applied enables the investigation of the time-varying effect of additives, in this case thiourea and chlorides, assisting the electroplating of copper.

1. Introduction

Electrorefining (ER) is the process of choice to purify copper [1]. Two main demands are driving this process to its limits. Primary, the need for urban mining, introducing different feed material into the process [2,3]. Secondary, the pressure to increase productivity. A relevant production problem in the ER industry is the formation of nodules on the copper cathodes [4–7]. This unwanted morphology can entrap electrolyte, hence, it is a main source of impurities in the copper and can cause process short circuits [6]. The origin of nodulation was frequently discussed in previous literature by Chen and Dutrizac [4,8,9] and others [5,6,10]. Two dominant processes could be identified for the nodular growth on copper cathodes. First of all, nodulation can be caused by particles in the electrolyte [5,8,9,11–13]. These particles, when attached to the cathode surface, serve as nucleation point. A second possibility for the formation of nodules arises from the equilibrium between current density and additive concentration, studied thoroughly by Winand et al. [14] and others [6,15–18]. Winand's investigation revealed the importance of an optimal balance between the operating current density (compared to the limiting current density) and the regulating additives, described by Plieth [15] as a stop-and-go process. Whereas the right ER conditions result in a smooth copper cathode, other conditions lead to powdery or nodular growth. The findings of the study were summarized in the well known Winand diagram [14]. Several additives are used in ER processes. Common additives are chlorides, thiourea (TU) and animal glue [1,19]. The mechanism of the TU and the TU-chloride mixture on the process is complex and still under debate [16,20–26].

To the best of our knowledge, there is a lack of long term mechanistic research governing the copper reduction reaction in the presence of additives, such as TU.

2. Aims and objectives

The goal of this paper is to extend the understanding of the time-varying copper deposition in the presence of TU in electrorefining electrolyte containing industrial copper concentrations [1,27].

In our previous studies [28,29], we combined operando Odd Random Phase Electrochemical Impedance Spectroscopy (ORP-EIS) with ion chromatography to analyze a simplified model ER system. The copper content was diluted and the experiments were performed in ambient temperature. The first study [28] revealed that the copper

* Corresponding author.
E-mail address: thomas.collet@vub.be (T. Collet).

https://doi.org/10.1016/j.electacta.2022.141412
Received 18 May 2022; Received in revised form 2 August 2022; Accepted 19 October 2022
Available online 1 November 2022
0013-4686/© 2022 Elsevier Ltd. All rights reserved.

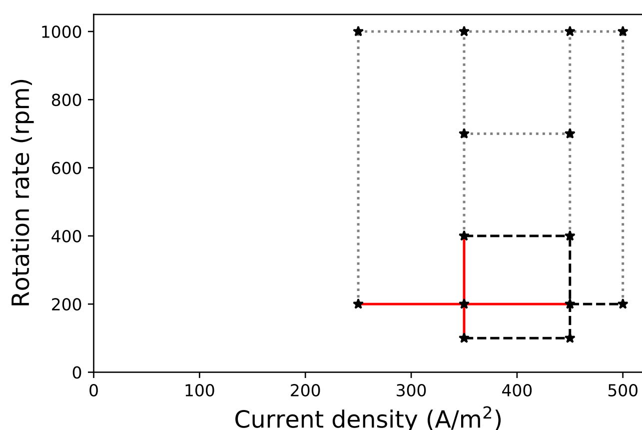

Fig. 1. Experimental design of the operando ORP-EIS experiments of the system without thiourea.

plating system in presence of TU shows time-varying behavior. The main origin of this time-variation is addressed to be the consumption of TU during the process [29].

The same experimental methodology as in our previous papers [28, 29] is now applied in a ER solution containing industrial copper concentrations, which is the final step towards experiments in an industrial environment. The measurements in this paper are performed in synthetic copper sulfate solutions, without contaminants and at industrial relevant current densities. Operando ORP-EIS [28,30–32] is used to characterize the copper plating process in operational mode. Operando ORP-EIS is an extension of our ORP-EIS technique [33–36], in which the input signal of the system consists out of DC current signal with an additional multisine signal [33]. The stochastic noise, non-linearities (NL) and non-stationarities (NS) of the system are quantified and analyzed. After assessing the presence of the NL and NS, the ORP-EIS technique enables the calculation of the Best Linear Time-Varying Approximation (BLTVA) [37–39] of a non-stationary system with mild non-linearities. The electrochemical impedance data is analyzed graphically [40,41], hereafter an Equivalent Electrical Circuit (EEC) is proposed to model the experimental data [41]. The model residual and the parameters errors are discussed before accepting the model as describing the data sufficiently [36]. Surface analysis is performed to analyze the effect of the TU activity on the copper cathode surface [15]. Initially, TU is absent to simplify the description of the system. Several current densities and mass transfer rates are used to study this base system. Afterwards a fixed current density is used to study the effect of TU on the copper plating.

3. Experimental

The following chemicals are used in the experiments performed for this paper: $CuSO_4.5H_2O$ (Merck p.a.), 95% H_2SO_4 (Fischer p.a.), KCl (UCB p.a.) and TU (Merck p.a.). KCl is used in the electrolyte to provide the necessary chloride ions because K_2SO_4 is used as salt bridge between the reference electrode and the copper sulfate solution. Milli-Q water is used for all solutions. The electrolyte used in this paper consistently contains 40 g/L of copper ions, 195 g/L H_2SO_4 and 0.045 g/L chloride ions, which are typical industrial ER electrolyte concentrations [1]. If TU is added, the concentrations are respectively 0.5 mg/L or 1.0 mg/L and are likewise industrially relevant [18,26,27]. A double walled cell is used as isothermic reactor vessel, set at 20 °C. The solution is deaerated with N_2 before every experiment and a N_2 blanket is applied during the measurements. A classic three-electrode configuration is used. A copper rotating disc electrode (RDE), with an active surface area of 0.13 cm^2, serves as working electrode. The rotation rate of the RDE is controlled by an Autolab RDE controller. The copper electrodes are mechanically polished before the experiments according to following grid-sizes: 800 μm, 500 μm, 9 μm, 3 μm and 1 μm and finalized with a chemical polishing step. A shunted SCE (+0.244 V vs NHE) with K_2SO_4 salt bridge provides a stable reference potential during the electrochemical experiments. To create a shunted SCE, the reference electrode (RE) is connected in parallel with a capacitor and a platinum wire (in series) which is inserted in the electrolyte together with the RE [42]. This RE setup allows the high frequencies to pass though the Pt wire, avoiding inconsistencies because of the RE's impedance. A Pt mesh is used as counter electrode.

The operando ORP-EIS excitation signal consists of the sum of a DC current and an ORP multisine [28–30]. The DC current drives the copper plating process (operando mode) [30], while the ORP multisine allows the calculation of the system's impedance (ORP-EIS) [33,34]. Measurements are performed with an in-house developed software and hardware setup. The frequency range 5 mHz–15 kHz is used. 20 periods are respectively measured to equalize the duration of the experiments to 4000 s or 1 h and 6 min, which is sufficiently long to simulate the ER process. Our previous research demonstrated that 80% of the initial TU concentration is consumed during a 1 h electroplating process [29]. The first period of every data set is omitted to avoid an increased transient effect, arising from the strong trend which is mainly present in the first period of the time domain data. Impedance data is then graphically analyzed and subsequently fitted with an Equivalent Electrical Circuit (EEC) to extract relevant parameters of the system [41]. Data modeling is performed with a Python 3.8 code. The weighted least squares are used as cost function and the residual is optimized with the Levenberg–Marquardt algorithm [33,34]. The parameter error is calculated from the Jacobian of the model. The quality of the data fit is assessed by the complex residual, the parameter error and the plausibility of the EEC [36].

The following experiment design is applied to study the system without TU. Four current densities, respectively 250 A/m^2, 350 A/m^2, 450 A/m^2 and 500 A/m^2, are combined with two diffusion layer thicknesses. The diffusion layer thickness is controlled by a rotating disk electrode. The first diffusion layer thickness is 0.031 mm (at 200 rpm) and simulates an industrial relevant diffusion layer thickness [43,44]. The other diffusion layer thickness is 0.014 mm (at 1000 rpm) and is applied to reduce the effect of diffusion on the ORP-EIS measurement and as such result in optimal conditions to study the system's kinetics. Three other RDE rotation rates are applied in the experiments at 350 A/m^2 and 450 A/m^2, respectively 100 rpm, 400 rpm and 700 rpm. This is done to visualize and analyze the effect of mass transport on our base system. The system containing TU is only studied at 350 A/m^2, with only the two rotation rates, 200 rpm and 1000 rpm.

The Leica DMi8 inverted microscope is used to analyze the copper cathode surface after plating.

4. Results and discussion

The result section of this paper is divided in two parts. The first part discusses the plating system without TU, also named the base system, which allows a thorough description of the copper plating system with high current densities and high copper concentrations. Afterwards, the knowledge gained from the base system is used to analyze the system with added TU.

The first step in analyzing impedance data is assessing the nuisance factors, which consist of the stochastic noise (N) and potentially non-stationarities (NS) and non-linearities (NL) [33–36]. If necessary, a Best Linear Time Varying Approximation (BLTVA) is calculated [37–39], to correct for the significant non-stationarities and take into account the non-linearities. This is followed by a graphical analysis [40] of the impedance data to obtain an initial physical explanation of the model. Hereafter, an Equivalent Electrical Circuit (EEC) is proposed and applied and the resulting model residual and model parameters are validated [36].

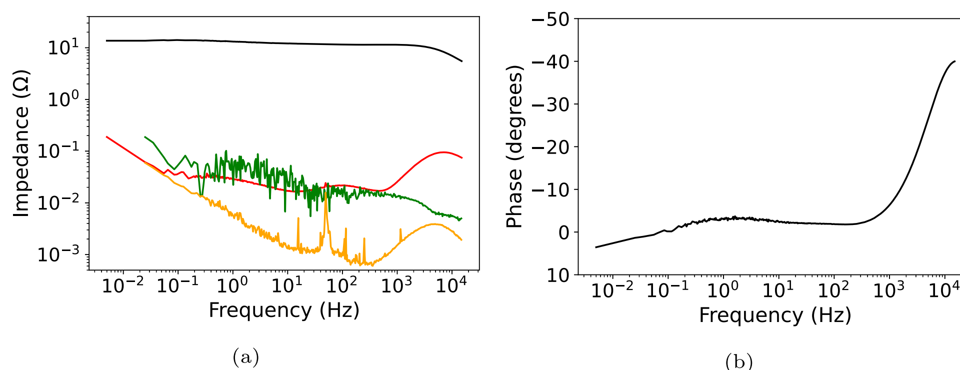

Fig. 2. Bode plots of operando ORP-EIS experiment performed in electrolyte containing 40 g/L of copper ions, 195 g/L H_2SO_4 and 0.095 g/L KCl, without TU. Copper plating executed at RDE with 200 rpm and 350 A/m^2. (a) Black line: Bode modulus plot, Green line: non-linearities, red line: non-stationarities: orange line: stochastic noise. (b) Black line: Bode phase plot.

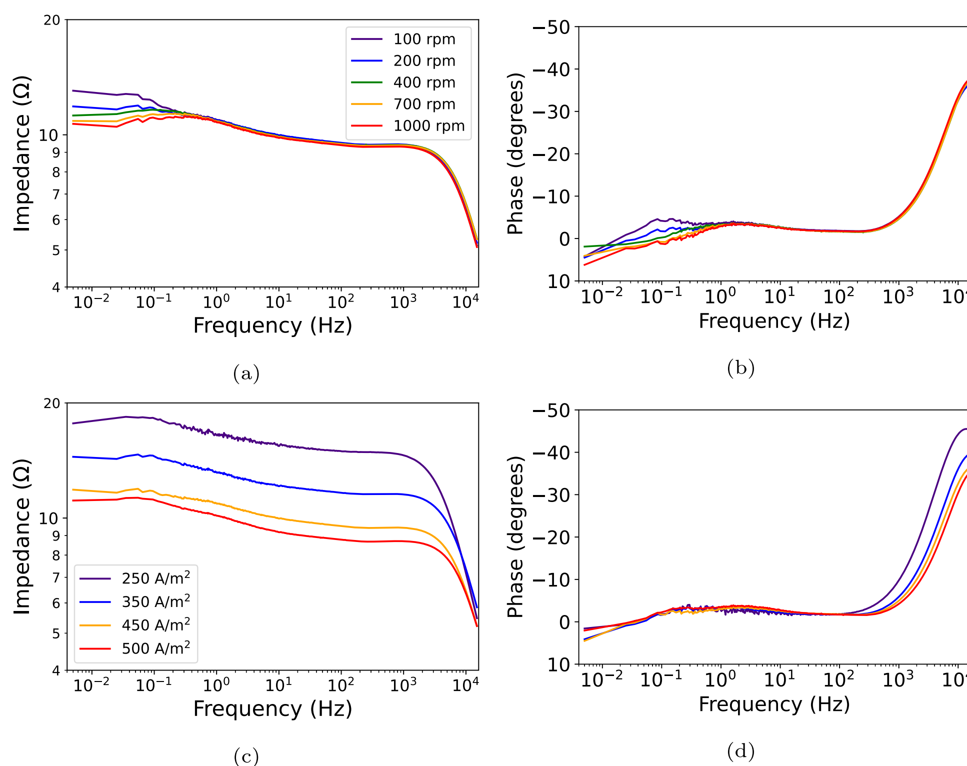

Fig. 3. Bode plots of operando ORP-EIS experiments performed in electrolyte containing 40 g/L of copper ions, 195 g/L H_2SO_4 and 0.095 g/L KCl, without thiourea. (a) Bode modulus plot, 450 A/m^2 and as a function of rotation rate. (b) Bode phase plot, 450 A/m^2 and as a function of rotation rate. (c) Bode modulus plot, 200 rpm and as a function of the DC current density. (d) Bode phase plot, 200 rpm and as a function of the DC current density.

4.1. Base system

The system without TU is studied with several current densities and rotations rates of the RDE. This allows a thorough description of the system's kinetics, mass transport and possible adsorption/desorption phenomena. The experimental design mentioned in the experimental part of this paper is displayed in Fig. 1. In this figure, the stars represent the parameter combinations used in the experiments. The red solid lines represent the experimental design with industrial relevant parameters [1]. The black dashed lines represent the experimental design at industrial relevant diffusion layer thicknesses, however, with elevated current densities. As the copper electrorefining industry aims to increase productivity, i.e., increase the current densities [45], these are relevant parameters for future production lines. The gray dotted lines are an extension of the experimental design towards conditions where diffusion becomes less important. This allows a complete study of the system under investigation and is again interesting for the future of copper electrorefining [46,47].

4.1.1. Analysis of the non-linearities and non-stationarities

The presence of NS or NL in the ORP-EIS measurements can be observed in the Bode modulus plots, as displayed in Fig. 2, which represents ORP-EIS data of an experiment performed at 200 rpm and 350 A/m^2. The black line represents the impedance modulus. The orange, red and green lines represent, respectively, the stochastic noise, the sum of the stochastic noise and the non-stationarities and the sum of the stochastic noise and the non-linearities.

A first difference between the impedance measurements with more complex plating conditions and the experiments with the simplified system [28] is the presence of non-linearities and non-stationarities in the solution without TU. However, these non-linearities and non-stationarities are considered minor due to the scale difference of two

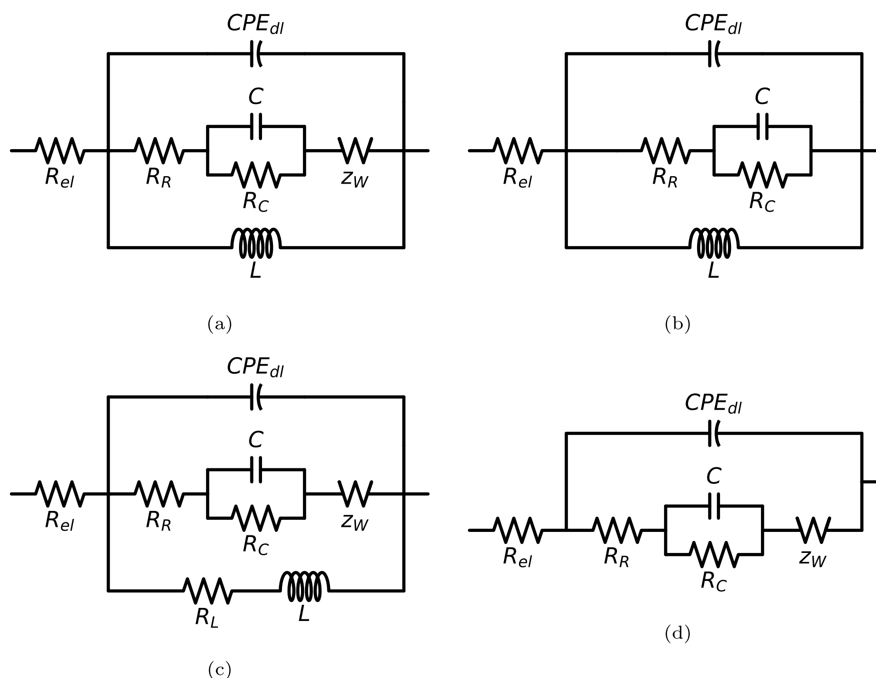

Fig. 4. Equivalent Electrical circuits used to fit the experimental ORP-EIS data. (a) Full circuit for the system without thiourea, which describes the electrolyte resistance, electrode double layer, kinetics, diffusion and adsorption/desorption. (b) Adapted circuit for the base system, the Warburg element is removed. (c) Full circuit for the system with thiourea, describing the electrolyte resistance, electrode double layer, kinetics, diffusion and adsorption/desertion. (d) Adapted circuit for the system with thiourea, the inductive branch is removed.

decades between the nuisance factors and the modulus. Fig. 2 is not used for interpretation of the ORP-EIS data. The scale difference between the nuisance factors and the Bode modulus prevent a good analysis of the modulus. Analysis of the impedance data is performed in the following subsection.

From above information, the substantiated decision is made to use the time-averaged impedance for measurements without TU. This data will be used for the graphical analysis [40].

4.1.2. Graphical analysis and EEC model

Fig. 3 represents Bode plots of the impedance data of experiments without TU. Figs. 3(a) and 3(b) represent experiments performed with a fixed DC current density, 450 A/m^2, as a function of the rotation rate. At 1000 rpm, three effects are observed in the Bode phase plot (Fig. 3(b)). The high frequency (HF) (15 000 Hz) capacitance represents the double layer capacitance on the electrode, the mid frequency (MF) capacitance (1 Hz) is not affected by the rotation rate and a low frequency (LF) inductance is present in the lowest frequencies. The MF capacitance was described in our previous paper as being part of a two-step electrode reaction with adsorbed intermediates [29]. The first reaction step is shown in Eq. (1) and the second step in Eq. (2). The inductance most probably arises from the adsorption and desorption of chloride [48–50]. Additionally, a LF capacitance (0.1 Hz) develops with decreasing rotation rate, introducing a fourth time constant. This LF capacitance most probably represents diffusion of the copper ions towards the electrode surface.

$$Cu^{2+} + e^- \rightarrow Cu^+ \tag{1}$$

$$Cu^+ + e^- \rightarrow Cu(s) \tag{2}$$

The experiments displayed in Figs. 3(c) and 3(d) are performed with a fixed rotation rate and a variable current density. The HF and MF capacitances, respectively 1000 Hz and 1 Hz in Fig. 3(d), vary as a function of the current density, as well as the HF resistance, 200 Hz in Fig. 3(c). From these observations, in combination with our previous knowledge, we can conclude that the HF resistance represents the reaction kinetics and that the MF capacitance is introduced by the two-step electrode reaction [41], as mentioned in previous paragraph. With low current densities (250 A/m^2), the diffusion part of the system seems to be negligible.

From above analysis, two EEC's are proposed to analyze the impedance data without TU. Fig. 4(a) displays the complete EEC, wherein R_{el} represents the electrolyte resistance, CPE_{dl} represents a non-unifrom double layer on the working electrode (Eq. (3)). R_R in series with the circuit $C//R_C$ is related to the two-step electrode reaction with adsorbed intermediate [29,41], Z_W represents diffusion by the general transmissive, finite Warburg (Eq. (4)). This Warburg consists out of three parameters. $Z_{W,R}$ represents the diffusion resistance, τ is an analytical value calculated from the diffusion layer thickness (δ) and the diffusion coefficient (D) (Eq. (5)) and ϕ represents general diffusion. If ϕ equals 0.5 the diffusion is uniform, any value below 0.5 represents non-uniform diffusion. L is the inductance. The inductance in an EEC is often coupled in series with a resistance R_L [41,50]. However, no R_L is added to the EECs used to model the ORP-EIS data from the system without TU because of a lack of inductive data points [28]. The inductance is applied to optimize the fit in the lower frequencies but the use of an overparameterized model is avoided by discarding the parameter R_L, as discussed in our first paper [28]. Fig. 4(b) represents the simplified EEC in which the diffusion is omitted.

$$CPE_{dl}(f) = \frac{1}{(j2\pi f)^{\alpha} Q} \tag{3}$$

$$Z_W(f) = Z_{W,R} \frac{\tanh(\tau j2\pi f)^{\phi}}{(\tau j2\pi f)^{\phi}} \tag{4}$$

$$\tau = \frac{\delta^2}{D} \tag{5}$$

4.1.3. Analysis of model residual and parameters

The two EEC's (Figs. 4(a) and 4(b)) discussed in previous subsection are used to model the experimental impedance of the system without TU. Fig. 5 displays the fitted Bode plots of the experiment without TU performed at 350 A/m^2 and 100 rpm, modeled with the EEC displayed in Fig. 4(a). The model is shown in cyan and the model residual as a

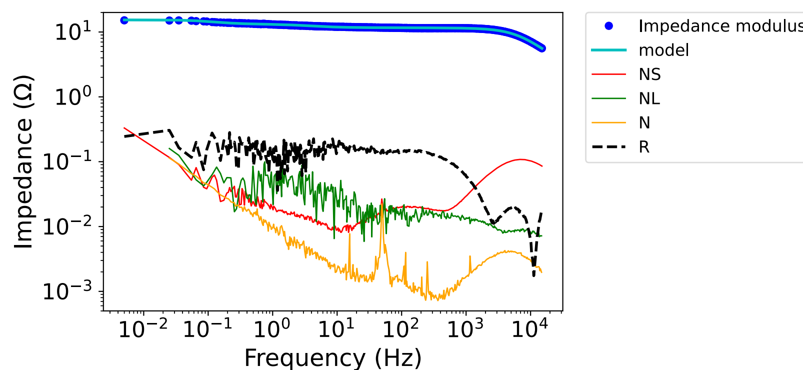

Fig. 5. Bode modulus plot of the operando ORP-EIS experiment performed at 100 rpm and 350 A/m^2 accompanied by its model. Blue dots: experimental data, cyan line: fit, black dashed line: residual of the fit, orange line: stochastic noise, green line: stochastic noise + non-linearities, red line: stochastic noise + non-stationarities.

black dashed line. The model residual is sufficiently low, i.e., near the data nuisance level, over the full frequency range. Hereby, the model is accepted as describing the data sufficiently.

The EIS data without TU is optimally fitted with circuit 1 (Fig. 4(a)), except the data of experiments performed at 250 A/m^2. The current density in these experiments is too low to have a distinguished diffusion process visible in the ORP-EIS data and therefore are modeled with circuit 2 (Fig. 4(b)).

The parameters used in the EEC are discussed next. The parameters are visualized as a function of the rotation rate (RPM), with the current density as variable (Fig. 6). Two parameters are fixed when performing the fit. τ is fixed to its analytical value and ϕ is fixed to 0.5 because we assume uniform diffusion [29].

The electrolyte resistance R_{el} is constant for all the experiments, only the experiment performed at 1000 rpm with 350 A/m^2 is an outlier, which is also noticed in the parameters R_R, Q, α, R_C and C_{dl}. Therefore, this point in the experimental design is neglected in the analysis. The charge transfer resistance (R_R) decreases as a function of the current density and is constant with rotation rate, which is logically expected.

The Q and α values are used to calculate the C_{dl} (Fig. 7), with the Brug equation [51] (Eq. (6)). C_{dl} is constant as a function of the rotation rate but shows minor changes as a function of the applied current density. This is expected, different current densities or different surface potentials change the double layer on the electrode surface [52].

The diffusion resistance $Z_{W,R}$ evolves inversely proportional as a function of the rotation rate, again logically expected. The mass transport towards the electrode surface is facilitated by an increased rotation rate.

Both the resistance R_C as the capacitance C decrease as a function of the current density, which proves the physical explanation of these parameters as being part of the two-step electrode reaction.

The inductance L shows no clear behavior. This probably originates from the low amount of data points where inductive behavior is seen.

$$C_{dl} = Q^{1/\alpha}\left(\frac{R_{el}R_R}{R_{el}+R_R}\right)^{\frac{(1-\alpha)}{\alpha}} \quad (6)$$

4.2. System containing thiourea

The EEC's applied in previous subsection are able to describe the copper plating reaction in high copper concentrations and with high current densities. In this subsection, well substantiated experimental conditions are chosen in a new experimental design (Fig. 8) to study the effect of TU in this system. The ORP-EIS experiments are performed at a fixed current density, i.e., 350 A/m^2, which simulates an industrial relevant processing rate [1,45]. Two variables are present in the experimental design, respectively the rotation rate and the TU concentration. The two extremes of the rotation rate applied in previous subsection, respectively 200 rpm and 1000 rpm, are also applied in these experiments. Additionally the TU concentration varies from 0, over 0.5, till 1 mg/L, again an industrial relevant parameter range [18,26,27].

4.2.1. Analysis of the non-linearities and non-stationarities

The Bode plots of the experiment performed at 200 rpm, with 0.5 mg/L TU are displayed in Fig. 9 to analyze the presence of non-linearities and non-stationarities. The difference between the impedance modulus and the non-stationarities and non-linearities is less than two decades. Therefore, the Best Linear Time Varying Approximation (BLTVA) of this measurement has to be considered instead of the time averaged ORP-EIS data. During the analysis of the output signal in the frequency domain [33,34], skirts are discovered, not only around the excited frequencies [35], representing a non-stationary behavior, but also around the present harmonics [38]. Hereby we can deduce that the system behaves non-stationary while containing non-stationary non-linearities. A novel approach was necessary to resolve the BLTVA from this system. This approach was developed by Hallemans et al. [38] and is applied in this work.

4.2.2. Graphical analysis and EEC model

The time varying impedance of the experiment performed with 1 mg/L TU and at 1000 rpm is visualized with Bode plots in Fig. 10. Two capacitances and a small inductance are observed in Fig. 10(b) at time interval zero. The HF capacitance is observed around 7000 Hz and the MF capacitance around 1 Hz. The HF capacitance shifts to lower frequencies as a function of time. Remarkably, both the MF capacitance and the inductance shift towards the opposite direction, towards higher frequencies over time and a third capacitance shows up in the LF region. The inductance is only visible in the initial and terminal phases of the BLTVAs. As discussed earlier, the HF capacitance arises from the electrode double layer and the MF capacitance from the two-step electrode reaction. The LF capacitance is assumed to be the diffusion and the inductance describes adsorption/desorption.

The HF resistance, observed around 1000 Hz in Fig. 10(a), decrease as a function of time. Likewise, the MF resistance, observed in Fig. 10(a) at 1 Hz when t = 200 s and at 5 Hz when t = 3620 s, decreases as well.

The EEC's used to model the BLTVAs are displayed in Figs. 4(c) and 4(d). The first and most complete model is used in the initial and final phases of the BLTVA. When the inductance is not visible in the data, the simplified circuit, Fig. 4(d), is used. The time intervals at which model 3 (Fig. 4(c)) or model 4 (Fig. 4(d)) are used differ, depending on the experimental conditions. The use of the two circuits is summarized when discussing the parameters extracted from the EEC's.

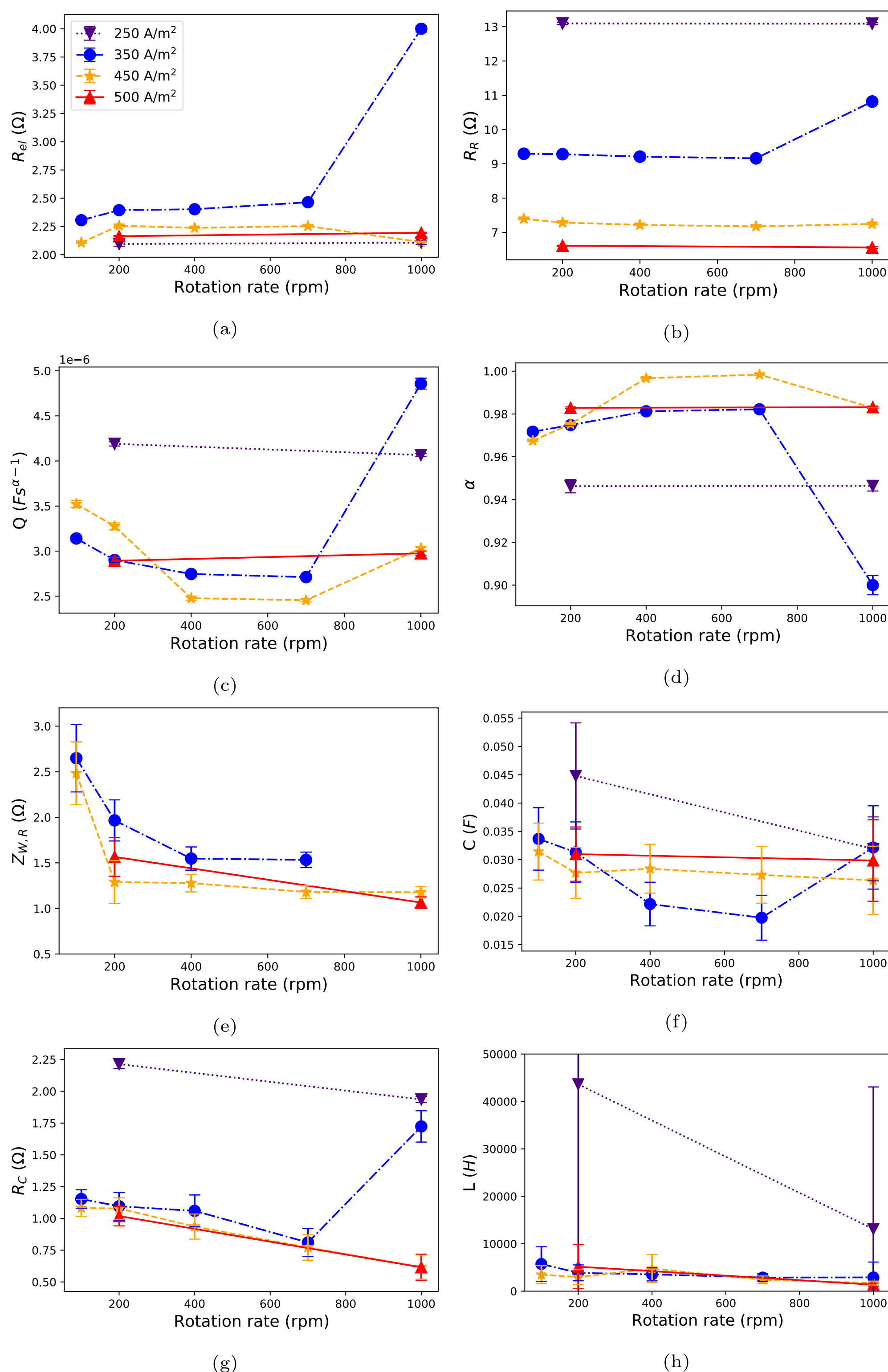

Fig. 6. Parameters extracted from the EEC's used to fit the time averaged ORP-EIS data without thiourea. (a) R_{el}, (b) R_R, (c) Q, (d) α, (e) $Z_{W,R}$, (f) C, (g) R_C (h) L. The error bars represent 95% confidence intervals.

4.2.3. Analysis of model residual and parameters

Three time intervals of a BLTVA (from the experiment performed with 0.5 mg/L TU and at 1000 rpm), respectively 200, 1340 and 3620 s, are displayed in Fig. 11 to analyze the EEC model fit and the residual of the fit. The noise level displayed in this figure differentiates from the stochastic noise displayed in the Bode plots from previous section. This noise is a total sum of the nuisance factors, being the stochastic noise and the non-linearities, estimated from the algorithm to calculate the BLTVA [38]. Initially (Fig. 11(a)) the model fit is near the noise level of the data. At an intermediate time interval (Fig. 11(b)) the data is described well but the model residual increases in the MF region, showing a minor discrepancy between the model and data. At the final stages of the ORP-EIS experiment (Fig. 11(c)), the model describes the full frequency range again very well.

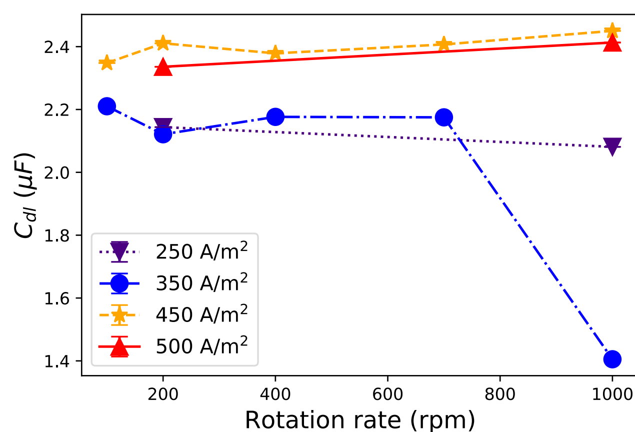

Fig. 7. Calculated double layer capacitance, using the Brug equation.

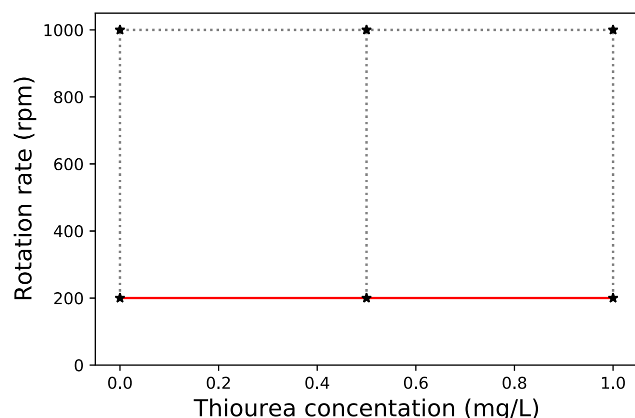

Fig. 8. Experimental design of the operando ORP-EIS experiments of the system with thiourea.

The parameters extracted from the experiments with TU are shown in Fig. 12. The electrolyte resistance (Fig. 12(a)) displays minor fluctuations around the same values as the R_{el} without TU. The charge transfer resistance (Fig. 12(b)) shows an interesting behavior. The presence of TU increases the initial R_R value from approximately 9.25 Ω without TU till approximately 10 Ω with TU, regardless of the TU concentration. This means that TU works in this system as an inhibitor of the copper reduction reaction. The fact that the starting values of the R_R parameter are lower for the different rotation rates and additive concentration is most likely introduced by the neglected first period in our measurements, because the first 200 s of the ORP-EIS measurement are not analyzed. After a certain amount of time the R_R values decrease and reach the same value as the R_R parameter extracted from the measurements without TU. A higher TU concentration results in a longer initial plateau of R_R. Additionally, the rotation rate and the decreasing rate of R_R are directly proportional. Increasing the rotation rate of the working electrode accelerates the downward trend of the charge transfer resistance. From our previous paper [29] we know that the charge transfer resistance is affected by the TU concentration. Ion chromatography experiments in combination with operando ORP-EIS experiments show that the electrochemical activity of TU is present in the beginning of every experiment but approaches zero as the TU concentration approaches zero (results not shown). If we link the TU activity to TU consumption, either on the cathode or the anode, we can conclude that the electrochemical consumption of TU in the process is limited by mass transport. However, the electrochemical activity of TU on the charge transfer resistance does not seem to be influenced by mass transport. Increased mass transport along the anode and cathode has always been seen as an important factor to increase the copper refining process [47,53]. In this system we can conclude that the increased mass transport also increases the TU consumption, which is a negative aspect towards the industrial process.

The trend of the measured potential of the ORP-EIS experiments is shown in Fig. 13. Again, the same experimental combination as in Fig. 12, containing three TU concentrations and two mass transfer rates, is displayed. The multisine potential data is averaged in blocks of 40 s, therefore the sine wave is still visible in the data. The initial potential of the experiments performed with TU is lower than the potential of the ORP-EIS plating experiment without TU. This same behavior is extracted out of the ORP-EIS data by the initial increase in parameter R_R. The potential varies as a function of time to the potential value of the ORP-EIS experiment performed without TU. The rate with which the zero TU potential is reached depends on the rotation rate and presence of initial TU concentration. The faster the rotation rate, the faster the zero TU potential is reached. The more initial TU is present in the electrolyte the slower the zero TU potential is reached. This is also observed by the time-variation in the R_R parameter.

The α (Fig. 12(d)) parameter of all the experiments starts between 0.90 and 0.96, increases as a function of time and approaches one. At the same time instance as the R_R parameter reaches its minimal value, the α parameter reaches its maximum value, after which its starts to decrease. As the α parameter is often regarded as a measure for surface uniformity [54] and we assume that the moment the R_R value reaches its minimal steady state value is the moment the TU activity drops to zero, we can conclude that the TU presence and consumption on the working electrode makes the electrode surface more uniform. Additionally, the moment the TU activity drops to zero, a decrease in the α parameter is observed.

The parameters Q and α, which are part of the CPE, are used to calculate the capacitance of the double layer C_{dl} (Fig. 12(h)) from the Brug equation [51], Eq. (6). This equation uses four EEC parameters R_{el}, R_R, Q and α to calculate the effective double layer capacitance. When the electrolyte contains 0.5 mg/L TU, the C_{dl} value start to increase at approximately the same moment that the R_R value reaches its steady state low value. The C_{dl} value of experiments which contain 1 mg/L TU show a totally different trend, which is not yet fully understood.

Parameter R_C (Fig. 12(e)) is very low for the four systems in the initial time intervals. After parameter R_R reaches its minimal value, R_C starts to increase. Hereby, it is possible to deduce that the initial reaction mechanism, in the presence of an abundant amount of TU, has one dominant or rate determining step. This rate determining step is most probably the step from cupric to cuprous (Eq. (1)) [55,56]. From the moment that TU is consumed, the reaction mechanism changes from a two-step reduction reaction with one charge transfer limiting step to a mechanism in which both steps are important. This mechanism is significantly different than the mechanism of the base system. Hereby, it is possible to conclude that the history of the electrolyte has a large impact on the copper plating mechanism [29]. The C parameter shows similar behavior as the α parameter. Initially showing an increase till a maximum value, after which the C parameter decreases. Unfortunately, the maxima of this parameter do not coincide with other changes in the other parameters and the parameter C is difficult to interpret physically.

$Z_{W,R}$ (Fig. 12(g)) displays different behavior depending on the rotation rate and initial TU concentration. No clear trend, neither correlations are observed.

The parameters L and R_L are displayed in Fig. 14. At low rotation rate, the inductance and R_L are present longer in the initial time intervals, till 380 s when 0.5 mg/L TU is present and till 1900 s if 1 mg/L TU is present. Increasing the rotation rate reduces the presence of the inductance and R_L in the initial time intervals, till 0 s for 0.5 mg/L and till 1330 s for 1 mg/L TU, but the inductance reappears in the final time intervals. It is possible to conclude that both the TU concentration

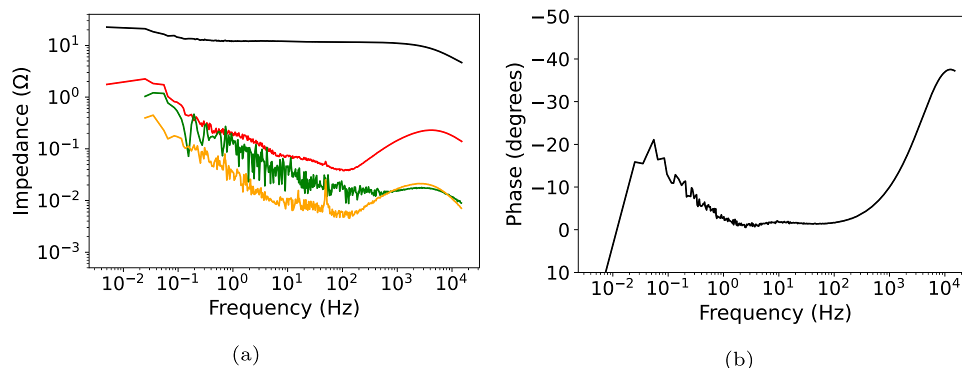

Fig. 9. Bode plots of operando ORP-EIS experiment performed in electrolyte containing 40 g/L of copper ions, 195 g/L H_2SO_4 and 0.095 g/L KCl, with 0.5 mg/L TU. Copper plating executed at RDE with 200 rpm and 350 A/m^2. (a) Black line: Bode modulus plot, Green line: non-linearities, red line: non-stationarities: orange line: stochastic noise. (b) Black line: Bode phase plot.

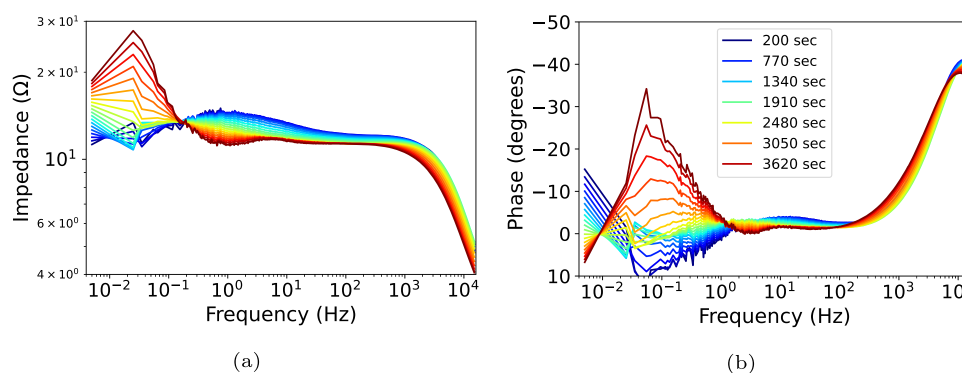

Fig. 10. BLTVA of the ORP-EIS experiment performed at 350 A/m^2 and 1000 rpm, with 1 mg/L TU. Darkblue = 200 s, darkred = 3620 s.

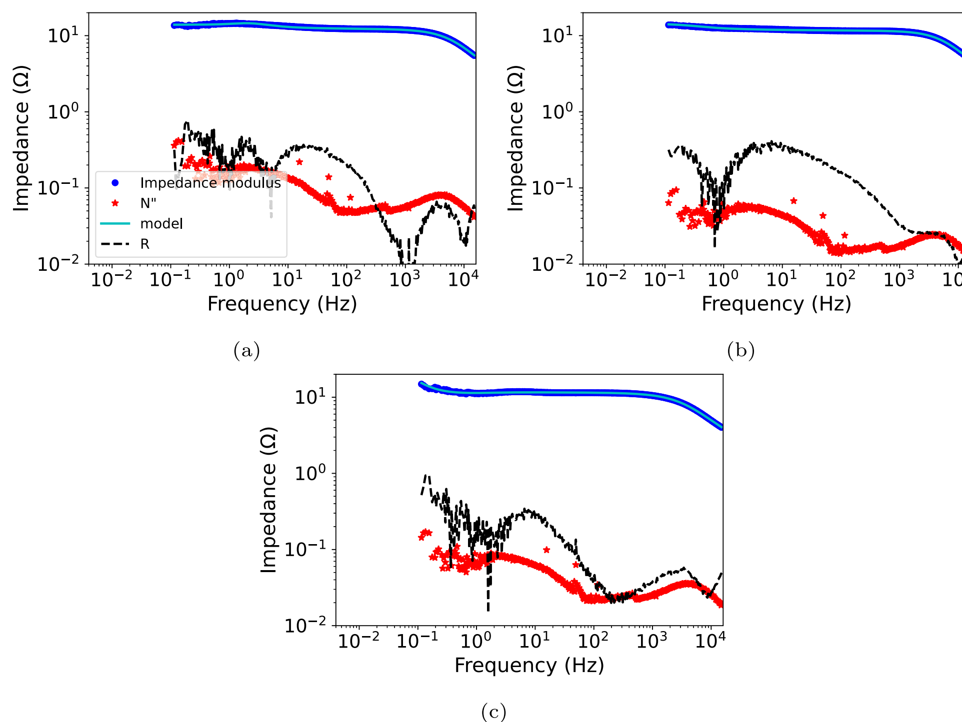

Fig. 11. modeled BLTVA, Bode modulus plots of the experiment performed at 1000 rpm with 0.5 mg/L TU. Blue dots: experimental data, cyan line: fit, black dashed line: residual of the fit, red stars: total nuisance. (a) 200 s, (b) 1340 s, (c) 3620 s.

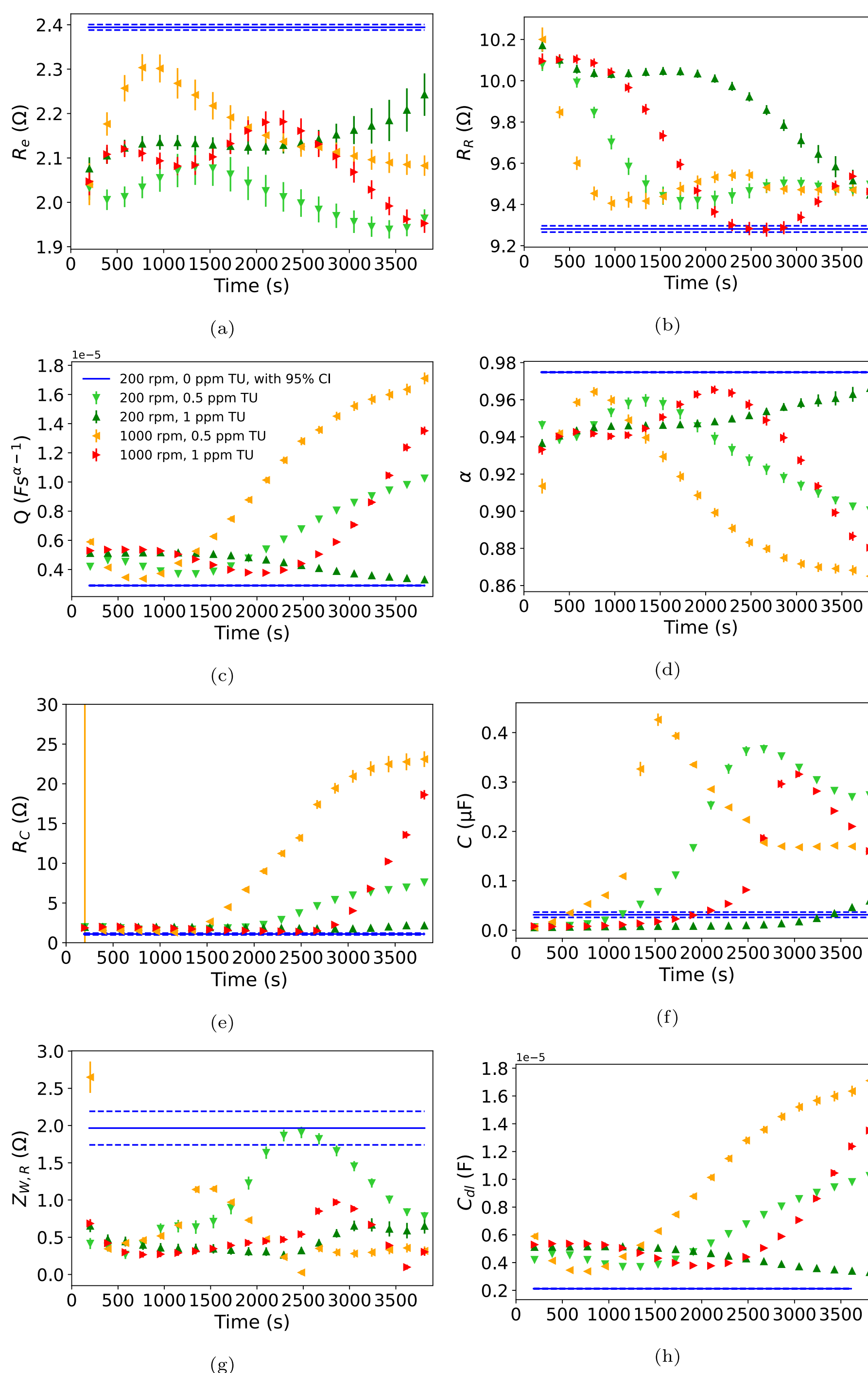

Fig. 12. Parameters extracted from fitting the BLTVAs from ORP-EIS data with thiourea. Blue ○: 200 rpm and without thiourea. Light green ▽: 200 rpm and with 0.5 mg/L thiourea. Dark green △: 200 rpm and with 1 mg/L thiourea. Orange ◁: 1000 rpm and with 0.5 mg/L thiourea. Red ▷ 1000 rpm and with 1 mg/L thiourea.

as the rotation rate are variables affecting the adsorption/desorption mechanism. A physical explanation of the parameters R_l and L is unfortunately very difficult and often neglected in electrochemical papers. With decreasing TU activity, the parameters R_L and L become larger, a larger L is observed at lower frequencies in the EIS data and at a certain moment the inductive data past below the lowest measured frequency. This explains why the R_L and L parameter values are not observed at all the time intervals. The increase of L and R_L in the initial time intervals of plating is to the best of our knowledge not yet observed in literature. No correlation is observed between the parameters L and R_L and the double layer capacitance C_{dl}, which is expected if this increase would derive from an evolution in adsorbed elements on the cathode surface. Unfortunately the initial increase of the inductive parameters L and R_L is still unclear. The decrease of this parameters can be interpret logically by the decrease in TU concentration but is again not correlated with other EEC parameters. Gabrielli [48–50] developed a physical model to describe the complete copper plating system, containing: kinetics, adsorption, etc. Nevertheless, a physical model is avoided in this work because of the numerous parameters involved in such a model and the unavoidable large parameter error [57].

4.2.4. Surface analysis

Microscopy images of the RDE surface as a function of the plating time are displayed in Fig. 15, the plating parameters are 1000 rpm and

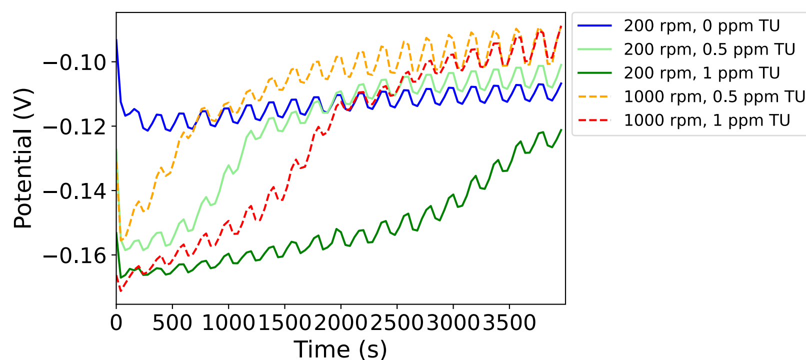

Fig. 13. The measured potential of the ORP-EIS experiments as a function of time, averaged in time intervals of 40 s. Blue: 200 rpm and no thiourea. Light green: 200 rpm and 0.5 mg/L thiourea. Green: 200 rpm and 1 mg/L thiourea. Orange: 1000 rpm and 0.5 mg/L thiourea. Red: 1000 rpm and 1 ppm TU.

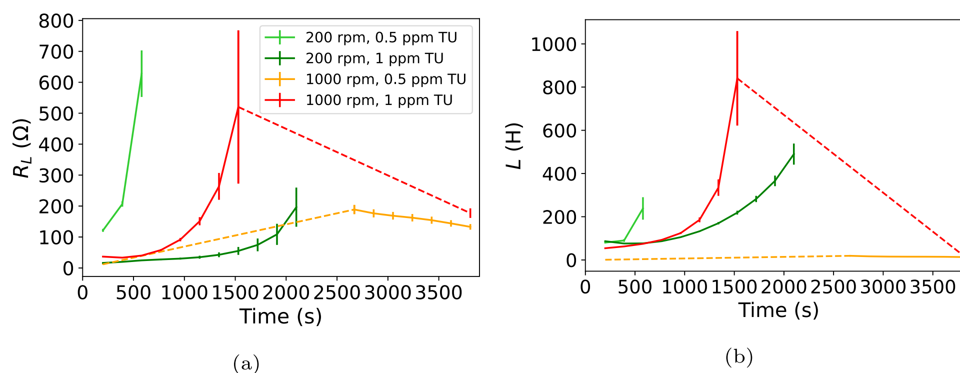

Fig. 14. Parameters R_L and L extracted from fitting the BLTVAs from ORP-EIS data with thiourea. The error bars represent 95% confidence intervals.

350 A/m^2. Fig. 15(a) shows the RDE surface after a short (960 s) plating time. At this time interval the charge transfer resistance is still at its initial value and a relative homogeneous and flat surface, containing minor roughness, is observed. When the TU activity and concentration is near 0 (after 2160 s), the copper surface exhibits an increased roughness, Fig. 15(b). This surface roughening is accompanied by the decrease in charge transfer resistance. Hereby it is possible to conclude that the inhibiting effect of the TU-Cl additive mixture has a positive effect on the morphology of the deposited copper on the cathode surface. Unfortunately, The moment microscopic roughness increases on the cathode surface, the α values extracted from fitting the operando ORP-EIS still increase. This observation indicates the complexity of the α parameter. Several mechanisms are stated to explain the presence of frequency dispersion [54,58–60] and surface roughness is one of them. The reaction rate distribution of a two-step reaction mechanism with adsorbed intermediates gives also rise to frequency dispersion [59] and this is a possible explanation for the discrepancy between the parameter α and the microscopic roughness of the cathode surface. The α parameter which initially was linked to surface roughness seems to be coupled more with the reaction kinetics than the homogeneity of the cathode surface.

4.2.5. Remarks

A physical explanation of the time-variation of the adsorption/desorption and diffusion parameters (L, R_L and $Z_{W,R}$) is not possible yet. Operando ORP-EIS experiments with a different input signal are necessary to study the effect of TU on copper plating in the lower frequencies. This new input signal optimally starts from lower frequencies and as such lengthen the experimental duration significantly. For example: an input signal with 1 mHz as lowest frequency increases the experimental duration by factor of five. As it is not possible yet to lower the frequency range without increasing the measuring time, developing an algorithm which allows the calculation of a BLTVA with a low amount of periods will gain importance in this research.

5. Conclusion

The operando ORP-EIS technique in combination with the algorithms to estimate the BLTVA is applied successfully in more complex conditions, containing industrial copper concentrations, to study the copper reduction reaction with the aid of common electrorefining additives.

The presence of a mid frequency capacitance as part of a two-step electrode reaction, which previously was assumed to be present, could be visualized and modeled in this paper.

The effect of plating time and TU consumption is clearly observed by several EEC parameters: the charge transfer resistance (R_R), α, R_C, C and C_{dl}. In the system under investigation in this paper, TU works as an inhibitor, increasing the charge transfer resistance. As a function of time, this resistance decreases till it reaches the initial charge transfer resistance value of the system without TU, thus the TU activity becomes zero. Nevertheless, the initial presence of TU in the electrolyte has an influence on other system parameters while the TU activity is zero. The α and C_{dl} parameter are heavily influenced by the initial presence of TU. Hereby it is assumable that reaction products of the TU consumption are still present in the electrolyte and affect the cathode double layer. Additionally, in the system which never contained TU and the system containing TU the copper deposition is observed as a two-step reduction reaction with one charge transfer limiting step. The moment the TU activity reaches zero, the second step of the two-step reduction reaction seems to become more important and the reaction kinetics is presumably controlled by the two reaction steps.

The history of the electrolyte, the presence of reaction products from the TU consumption in the case of this paper, has a large impact on the

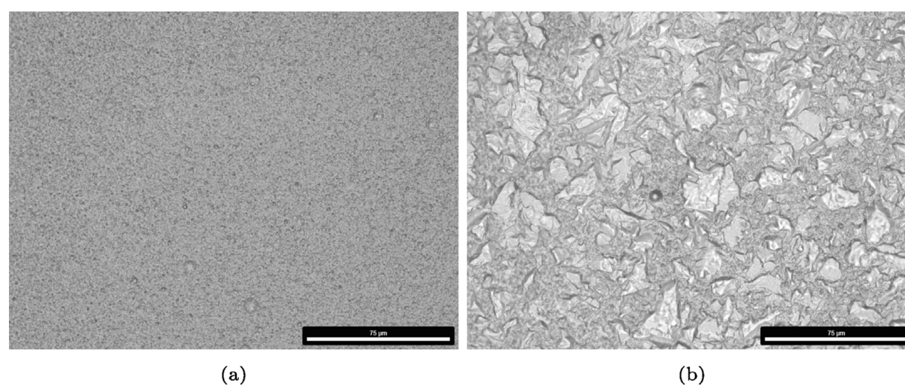

Fig. 15. Microscopy images of an RDE surface after copper plating with initial aid of thiourea, 350 A/m^2 and 1000 rpm. (a) after 960 s, (b) after 2160 s.

copper deposition mechanism. The cathode double layer, as well as the two-step deposition are influenced significantly by the initial presence of TU.

Optical microscopy proves the positive effect of the TU-Cl additive mixture on the copper cathode surface. The moment that the TU activity reaches zero, the cathode surface exhibits a higher roughness.

Unfortunately, the behavior of certain system elements (adsorption, diffusion, etc.) as a function of the TU concentration cannot be explained yet. Nevertheless, the effect of TU on the copper reduction reaction is shown, as well as some effects on the cathode surface. This information is a good starting point for industrial experiments.

CRediT authorship contribution statement

Thomas Collet: Conceptualization, Methodology, Software, Formal analysis, Investigation, Writing – original draft, Visualization. **Benny Wouters:** Methodology, Software, Formal analysis, Resources, Writing – review & editing. **Noël Hallemans:** Methodology, Software, Writing – review & editing. **Kristof Ramharter:** Writing – review & editing. **John Lataire:** Methodology, Writing – review & editing. **Annick Hubin:** Supervision, Writing – review & editing.

Declaration of competing interest

The authors declare that they have no known competing financial interests or personal relationships that could have appeared to influence the work reported in this paper.

Data availability

The authors do not have permission to share data.

Acknowledgments

This research is financially supported by Flanders Innovation and Entrepreneurship, Belgium (VLAIO grant HBC.2017.0212) and Aurubis Olen NV.

References

[1] M. Schlessinger, M. King, K. Sole, W. Davenport, Extractive metallurgy of copper, 2011.
[2] O. Forsén, J. Aromaa, M. Lundström, Primary copper smelter and refinery as a recycling plant—a system integrated approach to estimate secondary raw material tolerance, Recycling 2 (4) (2017) 19.
[3] F. Verbruggen, P. Ostermeyer, L. Bonin, A. Prévoteau, K. Marcoen, T. Hauffman, T. Hennebel, K. Rabaey, M.S. Moats, Electrochemical codeposition of arsenic from acidic copper sulfate baths: The implications for sustainable copper electrometallurgy, Miner. Eng. 176 (2022) 107312.
[4] J. Dutrizac, A mineralogical study of nodulated copper cathodes, in: Proc. COPPER 99 Int. Conf., 1999, pp. 383–403.
[5] Z. Mubarok, Analysis of industrial nodulated cathodes from Atlantic Copper and New Boliden, World Metall.-Erzmetall: Int. Fachzeitschrift Metall. 58 (2005).
[6] J. Bauer, M. Moats, Nodule formation on copper electrodeposits in the rotating cylinder hull cell, Metall. Mater. Trans. B (2022) 1–10.
[7] M.R. Shojaei, G.R. Khayati, S.M.J. Korasani, R.K. Harnashki, Investigating the nodulation mechanism of copper cathode based on microscopic approach: As a punch failure factor, Eng. Fail. Anal. (2021) 105970.
[8] T. Chen, J. Dutrizac, The mineralogy of copper electrorefining, JoM 42 (8) (1990) 39–44.
[9] T. Chen, J. Dutrizac, Mineralogical characterization of a copper anode and the anode slimes from the La Caridad copper refinery of Mexicana de Cobre, Metall. Mater. Trans. B 36 (2) (2005) 229–240.
[10] N. Okamoto, S. Takahashi, T. Saito, K. Kondo, Formation factor of nodule by copper electrodeposition, ECS Trans. 16 (22) (2009) 49.
[11] W. Zeng, S. Wang, M.L. Free, Experimental studies of the effects of anode composition and process parameters on anode slime adhesion and cathode copper purity by performing copper electrorefining in a pilot-scale cell, Metall. Mater. Trans. B 47 (5) (2016) 3178–3191.
[12] C.A. Moller, M. Bayanmunkh, B. Friedrich, Influence of As, Sb, Bi and O on copper anode behaviour–part 2: Anode dissolution behaviour and anode sludge generation, Erzmetall: World Metall. 62 (1) (2009) 6.
[13] C.A. Moller, M. Bayanmunkh, B. Friedrich, Influence of As, Sb, Bi and O on copper anode behaviour–part 3: Elemental distribution, Erzmetall: World Metall. 62 (2) (2009) 70.
[14] R. Winand, Electrocrystallization-theory and applications, Hydrometallurgy 29 (1–3) (1992) 567–598.
[15] W. Plieth, Additives in the electrocrystallization process, Electrochim. Acta 37 (12) (1992) 2115–2121.
[16] A. Tarallo, L. Heerman, Influence of thiourea on the nucleation of copper on polycrystalline platinum, J. Appl. Electrochem. 29 (5) (1999) 585–591.
[17] M. Moats, A. Luyima, W. Cui, Examination of copper electrowinning smoothing agents. Part I: A review, Miner. Metall. Process. 33 (1) (2016) 7–13.
[18] Z. Mubarok, I. Filzwieser, P. Paschen, Electrochemical and metallographic characteri-zation of inhibitor variation in copper refining electrolysis, in: Proceedings of EMC, 2005, p. 1.
[19] T. Muhlare, D. Groot, The effect of electrolyte additives on cathode surface quality during copper electrorefining, J. South. Afr. Inst. Min. Metall. 111 (5) (2011) 371–378.
[20] B. Veilleux, A. Lafront, E. Ghali, Effect of thiourea on nodulation during copper electrorefining using scaled industrial cells, Can. Metall. Q. 40 (3) (2001) 343–354.
[21] S. Jin, E. Ghali, Effects of gelatine, thiourea and chloride ion on the copper cathode polarisation behaviour in acidic copper sulphate at 65 ° C, Metall. Mater. Trans. B 32B (2001) 887–893.
[22] M. Peykova, E. Michailova, D. Stoychev, A. Milchev, Galvanostatic studies of the nucleation and growth kinetics of copper in the presence of surfactants, Electrochim. Acta 40 (16) (1995) 2595–2601.
[23] N. Tantavichet, M. Pritzker, Effect of plating mode, thiourea and chloride on the morphology of copper deposits produced in acidic sulphate solutions, Electrochim. Acta 50 (2005) 1849–11861.
[24] M.S. Kang, S.K. Kim, K. Kim, J.J. Kim, The influence of thiourea on copper electrodeposition: Adsorbate identification and effect on electrochemical nucleation, Thin Solid Films 516 (12) (2008) 3761–3766.
[25] B. Tadesse, M. Horne, J. Addai-Mensah, The effect of thiourea, L(-) cysteine and glycine additives on the mechanisms and kinetics of copper electrodeposition, J. Appl. Electrochem. 43 (12) (2013) 1185–1195.
[26] J. Baumbach, H. Bombach, M. Stelter, Investigations of the behaviour of thiourea and alternative additives in copper electrorefining, in: Proceedings of EMC 2015, 1995, pp. 151–160.

[27] P. Los, A. Lukomska, S. Kowalska, M. Kwartnik, Laboratory and pilot scale tests of a new potential-controlled method of copper industrial electrolysis, J. Electrochem. Soc. 161 (10) (2014) D593.
[28] T. Collet, N. Hallemans, B. Wouters, K. Ramharter, J. Lataire, R. Pintelon, A. Hubin, An operando ORP-EIS study of the copper reduction reaction supported by thiourea and chlorides as electrorefining additives, Electrochim. Acta (2021) 138762.
[29] T. Collet, B. Wouters, S. Eelink, K. Ramharter, A. Hubin, under revision, J. Electroanal. Soc. (2022) 1.
[30] M.D. Havigh, B. Wouters, N. Hallemans, R. Claessens, J. Lataire, H. Terryn, A. Hubin, Operando odd random phase electrochemical impedance spectroscopy for in situ monitoring of the anodizing process, Electrochem. Commun. (2022) 107268.
[31] X. Zhu, N. Hallemans, B. Wouters, R. Claessens, J. Lataire, A. Hubin, Operando odd random phase electrochemical impedance spectroscopy as a promising tool for monitoring lithium-ion batteries during fast charging, J. Power Sources 544 (2022) 231852.
[32] N. Hallemans, W.D. Widanage, X. Zhu, S. Moharana, M. Rashid, A. Hubin, J. Lataire, Operando electrochemical impedance spectroscopy and its application to commercial Li-ion batteries, J. Power Sources 547 (2022) 232005.
[33] E. Van Gheem, R. Pintelon, J. Vereecken, J. Schoukens, A. Hubin, P. Verboven, O. Blajiev, Electrochemical impedance spectroscopy in the presence of non-linear distortions and non-stationary behaviour Part I: Theory and validation, Electrochim. Acta 49 (26) (2004) 4753–4762.
[34] Y. Van Ingelgem, E. Tourwé, O. Blajiev, R. Pintelon, A. Hubin, Advantages of odd random phase multisine electrochemical impedance measurements, Electroanalysis 21 (6) (2009) 730–739.
[35] T. Breugelmans, J. Lataire, T. Muselle, E. Tourwé, R. Pintelon, A. Hubin, Odd random phase multisine electrochemical impedance spectroscopy to quantify a non-stationary behaviour: Theory and validation by calculating an instantaneous impedance value, Electrochim. Acta 76 (2012) 375–382.
[36] L.F. Macía, M. Petrova, A. Hubin, ORP-EIS to study the time evolution of the [Fe(CN)6]3-/[Fe(CN)6]4- reaction due to adsorption at the electrochemical interface, J. Electroanal. Soc. 737 (2015) 46–53.
[37] N. Hallemans, R. Pintelon, X. Zhu, T. Collet, R. Claessens, B. Wouters, A. Hubin, J. Lataire, Detection, classification and quantification of nonlinear distortions in time-varying frequency response function measurements, IEEE Trans. Instrum. Meas. 70 (2021).
[38] N. Hallemans, R. Pintelon, E. Van Gheem, T. Collet, R. Claessens, B. Wouters, K. Ramharter, A. Hubin, J. Lataire, Best linear time-varying approximation of a general class of nonlinear time-varying systems, IEEE Trans. Instrum. Meas. (2021).
[39] N. Hallemans, R. Pintelon, X. Zhu, T. Collet, M.D. Havigh, B. Wouters, R.I. Revilla, R. Claessens, K. Ramharter, A. Hubin, et al., Trend removal in measurements of best linear time-varying approximations–with application to operando electrochemical impedance spectroscopy, IEEE Trans. Instrum. Meas. (2022).
[40] M.E. Orazem, N. Pébère, B. Tribollet, Enhanced graphical representation of electrochemical impedance data, J. Electrochem. Soc. 153 (4) (2006) B129.
[41] M.E. Orazem, B. Tribollet, Electrochemical impedance spectroscopy, 2008, 61–72, 173–181, 338–340.
[42] T.J. Smith, K.J. Stevenson, Reference electrodes, in: Handbook of Electrochemistry, Elsevier, 2007, pp. 73–110.
[43] A. Kemminger, Characterization and Optimization of the Electrolyte Flow in a Conventional Tankhouse Cell (Ph.D. thesis), University of Leoben, 2015.
[44] W. Zeng, S. Wang, M.L. Free, Experimental and simulation studies of electrolyte flow and slime particle transport in a pilot scale copper electrorefining cell, J. Electrochem. Soc. 163 (5) (2016) E111.
[45] E.P. Wiechmann, P. Aqueveque, G.A. Vidal, J.A. Henriquez, Contact system design to improve energy efficiency in copper electrowinning processes, IEEE Trans. Ind. Appl. 49 (6) (2013) 2461–2465.
[46] C. Wenzl, A. Filzwieser, S. Konetschnik, Mettop-BRX-technology—industrial application, in: TT Chen Honorary Symposium on Hydrometallurgy, Electrometallurgy and Materials Characterization, John Wiley & Sons, Inc. Hoboken, NJ, 2012, pp. 63–76.
[47] W. Zeng, S. Wang, M.L. Free, C.-J. Tang, R. Xiao, Y. Liang, Design and modeling of an innovative copper electrolytic cell, J. Electrochem. Soc. 165 (14) (2018) E798.
[48] C. Gabrielli, P. Moçotéguy, H. Perrot, R. Wiart, Mechanism of copper deposition in a sulphate bath containing chlorides, J. Electroanal. Soc. 572 (2) (2004) 367–375.
[49] C. Gabrielli, P. Moçotéguy, H. Perrot, D. Nieto-Sanz, A. Zdunek, A model for copper deposition in the damascene process, Electrochim. Acta 51 (2006) 1462–1472.
[50] C. Gabrielli, P. Moçotéguy, H. Perrot, D. Nieto-Sanz, A. Zdunek, An investigation of copper interconnect deposition bath ageing by electrochemical impedance spectroscopy, J. Appl. Electrochem. 38 (4) (2008) 457–468.
[51] G.J. Brug, A.L. van den Eeden, M. Sluyters-Rehbach, J.H. Sluyters, The analysis of electrode impedances complicated by the presence of a constant phase element, J. Electroanal. Soc. 176 (1984) 275–295.
[52] M.H. Mamme, S.L. Moors, H. Terryn, J. Deconinck, J. Ustarroz, F. De Proft, Atomistic insight into the electrochemical double layer of choline chloride–Urea deep eutectic solvents: Clustered interfacial structuring, J. Phys. Chem. Lett. 9 (21) (2018) 6296–6304.
[53] A. Filzwieser, K. Hein, G. Mori, Current density limitation and diffusion boundary layer calculation using CFD method, JOM 54 (4) (2002) 28–31.
[54] C.L. Alexander, B. Tribollet, M.E. Orazem, Contribution of surface distributions to constant-phase-element (CPE) behavior: 1. Influence of roughness, Electrochim. Acta 173 (2015) 416–424.
[55] E. Mattsson, J.O. Bockris, Galvanostatic studies of the kinetics of deposition and dissolution in the copper+ copper sulphate system, Trans. Faraday Soc. 55 (1959) 1586–1601.
[56] M. Degrez, R. Winand, Determination des parametres cinetiques de l'electrodeposition du cuivre a haute densite de courant. Cas des solutions sulfurique sans inhibiteur, Electrochim. Acta 29 (3) (1983) 365–372.
[57] A. Lasia, Remarks on ‘‘EIS and statistical analysis of copper electrodeposition accounting for multi-component transport and reactions’’, J. Electroanal. Soc. 605 (1) (2007) 77–79.
[58] C.L. Alexander, B. Tribollet, M.E. Orazem, Contribution of surface distributions to constant-phase-element (CPE) behavior: 2. Capacitance, Electrochim. Acta 188 (2016) 566–573.
[59] C.L. Alexander, B. Tribollet, V. Vivier, M.E. Orazem, Contribution of surface distributions to constant-phase-element (CPE) behavior: 3. Adsorbed intermediates, Electrochim. Acta 251 (2017) 99–108.
[60] A. Lasia, The origin of the constant phase element, J. Phys. Chem. Lett. 13 (2) (2022) 580–589.